

A MULTIMODAL BRAIN-ARM INTERFACE FOR OPERATION OF COMPLEX ROBOTIC SYSTEMS AND UPPER LIMB MOTOR RECOVERY

Michele Folgheraiter¹, Elsa Andrea Kirchner^{1,2}, Anett Seeland¹, Su Kyoung Kim^{1,2}
Mathias Jordan¹, Hendrik Woehrle¹, Bertold Bongardt¹, Steffen Schmidt¹
Jan Christian Albiez¹ and Frank Kirchner^{1,2}

¹German Research Center for Artificial Intelligence (DFKI), Robotics Innovation Center
Robert-Hooke-Strasse 5, D-28359 Bremen, Germany

²University of Bremen, Robotics Lab, Robert-Hooke-Strasse 5, D-28359 Bremen, Germany
{michele.folgheraiter, elsa.kirchner, anett.seeland, su.kyoung.kim, mathias.jordan, hendrik.woehrle}@dfki.de
{bertold.bongardt, steffen.schmidt, jan.albiez, frank.kirchner}@dfki.de

Keywords: Haptic Interface, Bio-Inspired Design, Brain-Computer Interface, Wearable Exoskeleton, Support Vector Machine, Adaptive Brain Reading Interface, Electroencephalogram, Lateralized Readiness Potential, Bereitschaftspotential.

Abstract: This work introduces the architecture of a novel brain-arm haptic interface usable to improve the operation of complex robotic systems, or to deliver a fine rehabilitation therapy to the human upper limb. The proposed control scheme combines different approaches from the areas of robotics, neuroscience and human-machine interaction in order to overcome the limitations of each single field. Via the adaptive Brain Reading Interface (aBRI) user movements are anticipated by classification of surface electroencephalographic data in a millisecond range. This information is afterwards integrated into the control strategy of a wearable exoskeleton in order to finely modulate its impedance and therefore to comply with the motion preparation of the user. Results showing the efficacy of the proposed control approach are presented for the single joint case.

1 INTRODUCTION

Service robotics systems are becoming more and more complex both from the manipulation and locomotion capabilities point of view. This inevitably brings new challenges for their control strategy, which nowadays on the one hand is still lacking a complete autonomy and on the other hand is constantly required to accomplish the intention of the human that is interacting or supervising the machine.

To improve the interaction between the machine and the human it is therefore necessary to develop proper interfaces that allow a bidirectional communication: namely interpret the will of the user and translate it into a proper command for the robot, and reflex to the user the perception of the environment that surrounds the robot.

Exoskeleton interfaces for the upper and lower limbs have gained increasing attention in the last decade. They can be employed in a wide range of

applications: as master devices for teleoperation, as haptic interfaces that mediate the interaction of the user with virtual objects, as physiotherapy tools, or as devices that enhance the strength of the user.

The ESA Exoskeleton (Schiele and van der Helm, 2006), developed at the European Space Agency, is an example of upper limb interface equipped with 16 Degrees Of Freedom (DOF), eight of which moved via a tendon-based system. The device is intended to allow astronauts inside the International Space Station (ISS) to teleoperate EUROBOT, a humanoid robot that will support *extravehicular activities* (EVA). Although some of the joints are not directly actuated, the overall arm-exoskeleton system is fully controllable. This is due to the parallel structure that is formed during the interaction between limb and the device.

At the department of Electrical Engineering, University of Washington, a third generation dual-arm (7 + 7 DOF) exoskeleton (Rosen et al., 2005) was developed on the base of anthropometric data. The system

is fixed to the floor via a special frame; each arm has seven single-axis revolute joints moved by cables and pulleys that transmit the forces from the actuators located in the robot base. A precise placement of the joint singularities in the periphery of the workspace guarantees high-force isotropy and avoids workspace restrictions at the same time.

The SARCOS MasterArm (from SARCOS Inc.) (Mistry et al., 2005) is a 7 DOF hydraulically actuated arm-exoskeleton. The system is hung up by a fixed platform and the user operates the device by holding it at the most distal joint. The shoulder in this case remains unconstrained, but is positioned such that the three rotation axes of the exoskeleton approximately intersect with the center of rotation of the articulation.

Another important field where exoskeletons can bring significant benefits is represented by rehabilitation. In particular the usage of robotic devices is suitable for the long-term therapy of patients with neurodegenerative diseases or trauma-inflicted impairments (Reinkensmeyer et al., 2001; Harwin et al., 2006).

Robotic rehabilitation is expected to allow therapeutic interventions that are tailored to patients' conditions, enabling repeatable training curricula, objectified assessment of progress, and can be used by patients independently. Neuro-plasticity, i.e., the reorganization of tissue in the central nervous system (Harwin et al., 2006), is a key motivation for robotic rehabilitation. Stimulation of the sensorimotor system with increased levels of proprioceptive input generated by robotic rehabilitation devices has been argued (Reinkensmeyer et al., 2004) to yield higher levels of functional recovery than those achieved by conventional approaches in some studies.

The *MANUS* system, initially developed at MIT, has been in daily operation since 1994 delivering therapy to stroke patients at the *Burke Rehabilitation Hospital* (Krebs et al., 2004). *MANUS* is a planar module which provides two translational degrees-of-freedom for elbow and forearm motion. The module is portable and consists of a direct-drive five bar-linkage SCARA (Selective Compliance Assembly Robot Arm). The system has been commercialized and is currently marketed by *Interactive Motion Technologies Inc.*

ARMin II is the second prototype of a robot for arm therapy applicable to train activities of daily living in the virtual reality, developed at ETH Zurich. *ARMin II* has a semi-exoskeletal (grounded) structure with seven active degrees of freedom, five adjustable segments to fit different user sizes, and is equipped with position and force sensors. The system is back-drivable and enables the implementation

of impedance or admittance-based patient cooperative control strategies via analysis of force and torque sensor data.

The analysis of brain activity for the purpose of rehabilitation is mainly realized by the application of Brain-Computer Interfaces (BCIs) to restore the ability to communicate, manipulate, or move (Wolpaw et al., 2002). One of the first BCIs was based on the detection of the ERP P300 (Farwell and Donchin, 1988) which is elicited in the brain whenever a seldom and important stimulus is processed (Squires et al., 1975). Similarly, brain activity related to movement preparation or the imagination of movement is used to directly control computer programs, machines, or prostheses by the use of BCIs. For that, analysis focuses on the detection of event-related synchronization (ERS) or desynchronization (ERD) in certain frequency bands of the EEG (Leeb et al., 2006) or ERPs that are related to movement preparation (Blankertz et al., 2006), like the BP or the LRP (Kornhuber and Deecke, 1965; Masaki et al., 2004).

Movement related potentials (such as BP/LRP), evoked during voluntary movement tasks, have been analyzed by several BCI research groups. For instance, Blankertz et al. showed that it is possible to distinguish single trials of left vs. right finger movement in a self-paced keyboard typing task (Blankertz et al., 2003; Krauledat et al., 2004). The data processing for every channel is done first by emphasizing the end of each window of length 1280 ms sampled at 100 Hz with a cosine function of the form

$$w(n) := 1 - \cos\left(\frac{n \cdot \pi}{128}\right) \quad \text{for } n = 0, \dots, 127, \quad (1)$$

since for a fast detection of the LRP always the last points in time of the extracted signal are most important. After that, a frequency filtering with a pass-band from 0.4 to 3.5 Hz and a subsampling to 20 Hz is applied. Then the last 4 data samples in each window are used as features and are classified by Regularized Fisher Discriminant. For a pseudo-online test in a feedback session, where subjects see the classifier output as a moving trace on a screen, sliding windows are extracted every 40 ms.

The data set generated by Blankertz et al. was also published for the NIPS*2001 (BCI) post-workshop Competition 2001 (Sajda et al., 2003) and analyzed by several other authors with different approaches. For example, Pires et al. filtered below 5 Hz and generated features using a regression model. These features were then classified with Linear Discriminant Analysis (Pires et al., 2007). In contrast Li et al. used the amplitude difference between left and right electrodes as features, after a filtering from 0 to 3 Hz. Subsequently spatial filtering is applied and features are

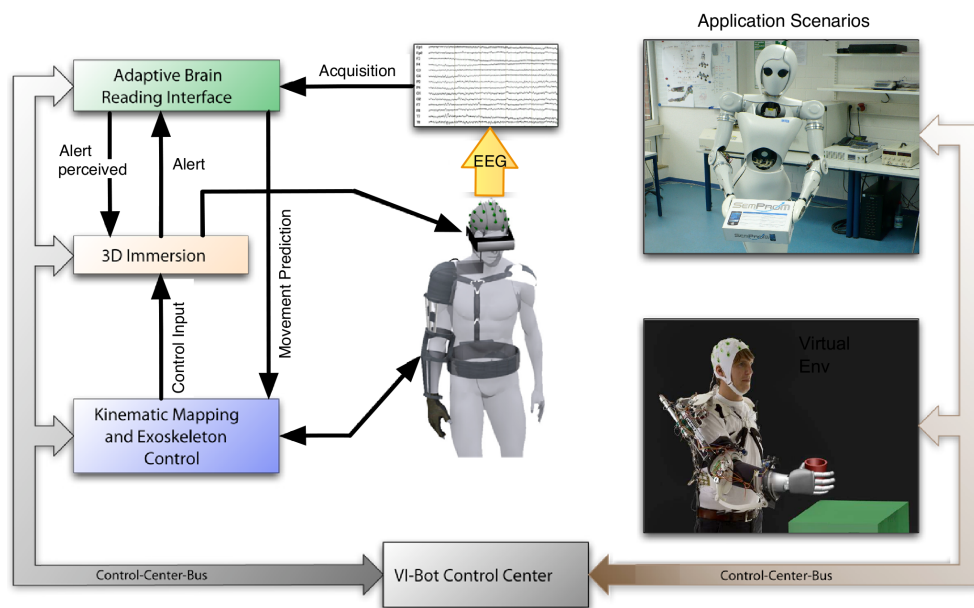


Figure 1: The Overall Control Framework Architecture.

classified with a perceptron. Furthermore they used additionally frequency features for the detection of ERD/ERS and improved classification performance (Li et al., 2004). Nevertheless both approaches were not tested in an online manner.

Beside the discrimination of right vs. left movement, it is in an online scenario of particular importance to detect the movement *per se*. For this purpose, Blankertz and colleagues outlined another classifier, which is tested in combination with the classifier performing the left-right movement discrimination. However, the authors admit, that further research has to be done to improve the distinctness of the classifier output (Blankertz et al., 2002).

2 THE MULTI-MODAL CONTROL ARCHITECTURE

One main goal of our project is to develop a multi-modal control interface that will enable a single human operator to control such complex robotic systems in an intuitive way. The interplay between a safe wearable exoskeleton, an adaptive Brain Reading Interface (aBRI), and a multipurpose virtual environment will lift the control of different robotic systems up to the next level, enabling to dissolve the boundaries between robot and operator, as well as combining the cognitive abilities of the human with the robustness of the robotic system. Figure 1 depicts the overall control scenario where the user, at the cen-

ter of the architecture, is wearing the three interfaces. This paper mainly focuses on the *exoskeleton* and the *aBRI*; the *3D-Immersion* and *Control Center* modules are therefore not described in detail. In particular, a control scheme is proposed that uses the information coming from the detection of movement preparation (Section 4) to modulate the behavior of the haptic interface and therefore to improve the interaction experience between the user and the robotic system. However, for the acquisition of the electroencephalogram (EEG), a virtualized scenario is used as explained in Section 4.2.

Due to the fact that the kinematics of the exoskeleton and its control system were tailored on the base of the anatomy and neurophysiology of the human limb (Section 3), such interface is also suitable for delivering a precise and customized rehabilitation therapy for the human arm.

In particular, we want to introduce an approach for the support of patients suffering from a partial lack of the control of their motor system. For several reasons, e.g., after an accident, it might be hard for a patient to move an injured limb properly with the required force and precision. To assist recovery of the patient, we want to apply a wearable exoskeleton whose functionality is based on a bio-inspired control strategy that allows a natural integration of predictions regarding the prepared movements of the patient. Pre-knowledge about movements allows the system to support the patient more accurately. The movement prediction is based on the on-line analy-

sis of brain activity. The integration of this information into the control architectures allows to support the patient even in situations where he or she cannot move his/her limb by him-/herself, but brain activity can still be measured. For this purpose, single trial online-detection of movement-related brain activity without knowing movement onset has to be accomplished. To achieve this, our framework for aBRI (Kirchner et al., 2009; Kirchner et al., 2010) was extended to allow movement prediction based on the detection of certain event related potentials (ERPs), i.e., the lateralized readiness potential (LRP) and the Bereitschaftspotential (BP) (Section 4), and integrated into the brain-arm interface. For best results several combinations of filters and their related data processing times are compared.

The brain-arm haptic interface will not only support the execution of the movement by reinforcing the strength, but also by supporting the patient for a precise trajectory execution. Due to the fact that the joint impedance is modulated via the integration of the movement preparation signal and the measurement of the exoskeleton-arm interaction forces, the system will always respond in a natural way according to the prepared user movement. The presence - at joint level - of different safety mechanisms (Folgheraiter et al., 2009c) will guarantee that the torque/force applied to the limb will be limited within a proper range. This is very important in order to avoid uncomfortable or even dangerous postures for the user.

3 EXOSKELETON INTERFACE - DESIGN AND CONTROL

The arm interface is a 9 DOF wearable exoskeleton designed to deliver a fine force feedback in three contact points with the user limb: shoulder, upper-arm, and forearm. The device is hydraulically as well as pneumatically actuated; the pump, compressor, and primary power supply are located outside the exoskeleton to avoid additional weight to the system.

In total there are seven actuated joints: five located in the shoulder/upper-arm and two in the forearm (Figure 2). Two additional passive joints allow the wrist supination-pronation, finally two adjustable links permit the adaptation of the shoulder and upper arm lengths to the specific user anthropometry.

The haptic interface is intended to be easily worn by the user due to the presence of adjustable strips and belts around the upper-body, upper arm, and wrist. During operation, all reaction forces are loaded on the

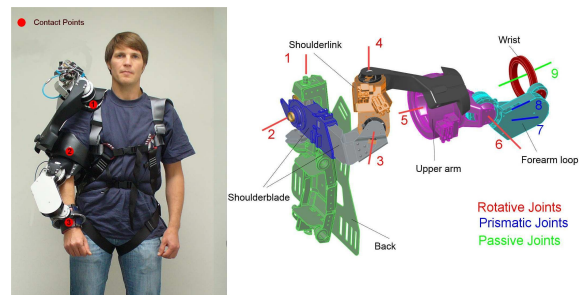


Figure 2: The 9-DOF arm exoskeleton.

back of the operator, therefore the weight of the system is not directly perceived on the limb. Although a big effort was dedicated to keep the structure as light as possible, at the moment the full prototype has a weight of 14 Kg, as thus for usage as rehabilitation tool needs to be supported by a tutor, which can be connected in the back part of it.

3.1 Exoskeleton Kinematics Design

To define the kinematic architecture of the exoskeleton, at first we modeled the human arm using a common notation from robotics, this enables us to easily combine the two systems in order to study the overall mobility. Figure 3 depicts, that the coupled arm-exoskeleton system shows different closed kinematics loops. This in general brings restriction to the movements of the limb, requesting a proper analysis of the combined system.

Through a series of simulations, and by the integration of real arm trajectories, it was possible to set the requirements to design the final device (Folgheraiter et al., 2009b), e.g., number and configuration of the DOF, angular range for each joint, optimal link dimensions, joint-articulation alignment, and maximum joint torque required. The kinematic architecture, depicted in Figure 3 (blue parts), includes a total of 9 DOF. Starting from the back connection toward the upper arm contact point (where $Ja5$ is located), the presence of 5 actuated DOF guaranty free mobility of the shoulder as well as the possibility to deliver a three-dimensional force feedback. From the upper-arm toward the forearm other 4 DOF allow the elbow flexion-extension and the forearm pronation-supination. To notice that the additional DOF that let the wrist flexion-extension are not consider in this study; this is due to the fact that the last contact point between the haptic interface and the arm is located before the wrist articulation.

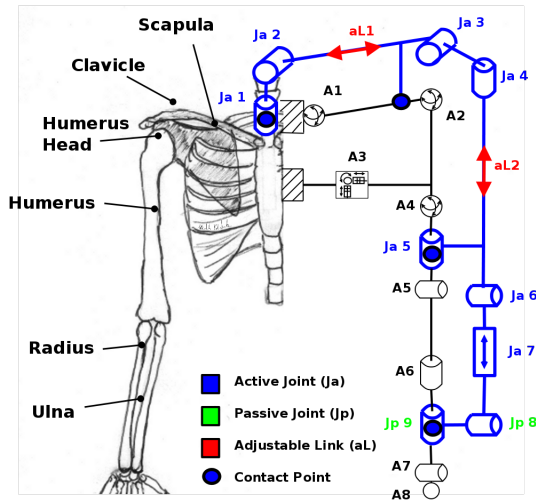


Figure 3: The simplified human arm kinematic model (right side in gray) combined with the exoskeleton model (in blue).

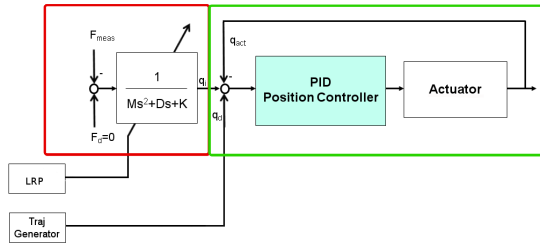


Figure 4: Exoskeleton single joint control scheme; (left square) force controller; (right square) cascade PID position controller

3.2 Single Joint Control System

This section focuses on the description of the single joint position/force controller. Both elements are based on classical controller approaches building the basis of the bio-inspired control scheme (Folgheraiter et al., 2009a), (Folgheraiter et al., 2009c) as well as the connection to the aBRI interface. Figure 4 shows a schematic of the low-level joint controller consisting of these two parts.

In Figure 4, the right square marks the cascade PID position controller, while the left square marks the part including the adaptive admittance controller. Within the position controller structure, q_d describes the desired actuator position given by a trajectory generator located in a superior part of the overall control system, and q_{act} is the actual actuator position. Results for single joint position control are shown in Section 5.1.

The force controller includes a variable admittance filter with a specified stiffness K , damping D ,

and inertia M , while q_i is the change in actuator reference position due to an error between the desired interaction force F_d and the measured force F_{meas} . The described force controller passively regulates the interaction force between the operator and the exoskeleton by introducing a mass-spring-damper relationship between q_i and F (Hogan, 1985). The transfer function of the admittance filter is given by the following equation:

$$q_i = \frac{1}{Ms^2 + Ds + K} \cdot (F_d - F_{meas}). \quad (2)$$

The resulting deviation q_i caused by a measured contact force F_{meas} has to be tracked by the subsequent position controller described before. Through adaptation of the three coefficients K , D , and M using the result of the movement preparation detection one can specify the reaction of the device to an occurring movement. Generally the stiffness K regulates the amplitude of interaction force for a given trajectory, while the damping factor D specifies whether more or less energy is to be dissipated during the movement. A verification of the effect of these two parameters to admittance filter characteristic is done in 5.1. The inertia factor M is neglected because the device should not propagate a virtual mass to the operator. If movement preparation is detected the values of K and D are adjusted using Equations 3 and 4, causing the exoskeleton to respond more or less sensitively to any given force input generated by operator movements.

$$K = K_{st} - (S_{LRP} \cdot \Delta K_m) \quad (3)$$

$$D = \begin{cases} D_{st} + (S_{LRP} \cdot \Delta D_m) & , S_{LRP} < \epsilon \\ D_{st} - \frac{1}{1-\epsilon} (S_{LRP} - \epsilon) \cdot \Delta D_m & , S_{LRP} \geq \epsilon \end{cases} \quad (4)$$

Equation 3, K_{st} is representing the stiffness coefficient when no preparation of movement (LRP and BP) is detected, $S_{LRP} \in [0, 1]$ is the score value the LRP detection algorithm provides to the exoskeleton control system, and ΔK_m is the maximum allowed change of stiffness due to a detected movement preparation. Further, in Equation 4, D_{st} is representing the damping coefficient in case of no movement preparation (LRP and BP) detection, ΔD_m is the maximum allowed change of damping ratio, while ϵ is representing a threshold the LRP score has to overcome to guarantee that a starting movement is quite possible. In the overall context ϵ is used to tune the force controller more sensitively according to the LRP detection algorithm. This means explicitly, that in case of low LRP scores, smaller than the threshold ϵ , the possibility of a movement of the operator is very low. In any case the stiffness is lowered by Equation 3 resulting in a higher sensitivity of the device to any given

input. By a parallel increase of the damping the device is reacting more conveniently.

If the LRP score overcomes the threshold, stiffness as well as damping are reduced, preparing the system to react instantaneously to an expected movement of the operator. Results of single joint admittance control using variable stiffness and damping are presented in Section 5.1.

4 aBRI INTERFACE - ARCHITECTURE AND METHODOLOGY

Most applications in the context of rehabilitation that make use of the EEG, namely brain activity recorded on the surface of the skull, are situated in the field of BCIs. Those interfaces serve to restore the ability of disabled patients to communicate (Wolpaw et al., 2002) by enabling them to control machines or computer programs by brain activity.

Our approach is not to use brain activity to directly control any devices, but to read the brain activity to gain insight into the human mental and/or cognitive state (Kirchner et al., 2009; Kirchner et al., 2010). The developed interface is called *adaptive Brain Reading Interface* (aBRI) and can be used to "inform" a control scenario about, e.g., warning processing of the user or, like in this application, the preparation to move a certain limb. In both cases, the aBRI will work in the background and does not require any cognitive resources of the user. The aBRI, utilized for movement prediction, is combined and linked via a bio-inspired control architecture with a wearable exoskeleton which together form the brain-arm haptic interface.

Before a movement is executed, it is planned by the brain. Especially directed movements, in comparison to, e.g., reflexes, are planned and controlled by the cortex. Several areas of the cortex are involved in motor planning. By detecting the activity of those brain areas it is possible to predict the occurrence of movement as well as which part of the body will be moved. As presented later on, movement onset prediction is done in real-time by single trial detection of ERPs called LRP and the earlier evoked BP (Kornhuber and Deecke, 1965; Balconi, 2009).

In comparison to the detection of changes in the frequency range of the EEG (Leeb et al., 2006), the detection of ERPs is possibly faster, since ERPs are temporally clearly differentiated brief events and especially in the case of the BP much earlier to detect. The BP, also called readiness potential (RP),

can be detected even seconds before the start of the movement though a differentiation between the side of movement e.g., right or left, and the part of the body, e.g. arm or leg, can only be predicted by the later evoked LRP which is the lateralized part of the RP. The LRP can be measured above certain parts of somatotopically organized brain areas to differentiate between periods of movement and rest of correspondent body areas.

Our approach therefore allows in principle not only to detect movement onset very early by detecting the BP but also to differentiate between the side of movement and certain parts of the body by detecting the LRP. We also believe that the detection of ERP components is less prone to artifacts possibly originating from muscle activity or noise induced by the exoskeleton, e.g., by hydraulic pumps or electronically controlled switches. Especially muscle artifacts are a major problem since the subject is not seated in a chair but is standing and therefore constantly moving slightly while wearing and using the exoskeleton. Since the chosen data processing for ERP detection needs only information in the very low frequency range (below 4 Hz), rigorous filtering can be applied that eliminates or at least strongly reduces the before mentioned artifacts.

The challenge of our approach is the detection of a rather weak signal of short duration at an unknown time point. Both, BP and LRP are about 10 to 100 times smaller in amplitude than the superimposed brain activity and can normally only be detected in average analysis (enhancing time-triggered ERP activity and reducing so-called activity-unrelated noise). For our approach, single trial EEG analysis in real time is needed that has to be fast to allow multiple testing for the occurrence of ERPs before the movement.

4.1 Framework

In this section, we present the architecture of our framework for the aBRI that is used to make a prediction whether an operator prepares to perform a movement or whether he does not. This prediction is integrated into the bio-inspired control architectures that controls the stiffness of the exoskeleton.

The framework is designed to classify single trial EEG epochs, which is a major requirement for various different application scenarios for *adaptive Brain Reading* (aBR) (Kirchner et al., 2009). Since a machine-learning based approach is used for single trial classification, the framework has to support various data preprocessing methods and training sessions of the underlying classifier.

Major requirements for the aBRI are, among oth-

ers, a high classification accuracy, modular design to facilitate the development process by rapid prototyping, different instances of possible data processing designs and evaluation of the used algorithms, as well as high performance for online data processing.

To fulfill these requirements, the data processing system is based on the Modular toolkit for Data Processing (Zito et al., 2008), which in turn is based on NumPy and SciPy (Jones et al., 2001) to perform the computations. These frameworks consist of C++ implementations of the mentioned algorithms with bindings to Python. Since the actual computationally intensive algorithms are realized as binary object code, the performance impairment of a scripting language does not account here significantly.

The framework is realized as a set of independent modules which are called *nodes*. Several nodes can be assembled to create *flows*, where the data is transferred from one node to the next one. Different especially time-critical nodes are realized in C++ and a channel-wise parallelization by using OpenMP.

The overall processing system is structured as follows (Figure 5 for an overview):

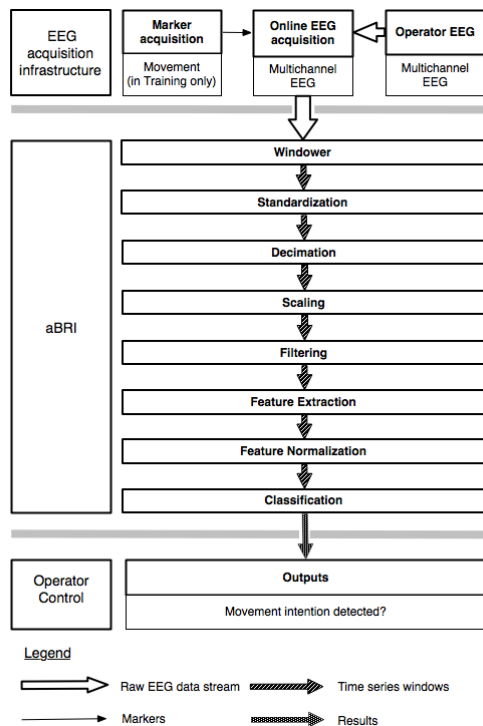


Figure 5: Data processing scheme.

EEG Acquisition. This module acquires the data from the EEG hardware and transfers it to the successive data processing modules. In this step, the data is a continuous stream of the raw signal data. An important point is the capability to automatically add markers to

the datastream to label special events for training sessions, e.g. when the operator starts to move or enters a specific position. A streaming of files which contain previously acquired EEG data is also possible.

Windowing. In this step, the raw EEG data stream is segmented into windows of the same shape (length of the signal frame) to extract instances which can be processed and classified independently of each other. This simplifies the successive computations since it allows to work always on instances of the same shape.

The process of extracting the time windows is called *windowing*. The framework is capable of using different methods for window generation, e.g. to generate training samples for classifier training and testing by using specified markers, or for online data processing in the real application scenario.

In the case of BP and LRP detection later on EEG data is segmented into windows of length of 1000 ms. Instances containing movement preparation were cut out with respect to a movement marker and instances containing no movement preparation were extracted during a rest period (Section 4.2).

Preprocessing and Feature Generation. Preprocessing refers to operations aimed at increasing the signal-to-noise ratio. It can be performed in several steps. In Figure 5, an example flow with several different data processing methods is shown.

Specifically in the flow which is used later on for the movement prediction, each window is standardized channel-wise (subtraction of the corresponding mean and division by the standard deviation). A decimation is applied afterwards with an anti-aliasing filter to reduce the sampling rate of the data from 5000 Hz to 20 Hz.

After that, the data is scaled with the function specified by Equation 1 from Section 1. The next processing step is another band pass filter with a narrow frequency band, which is applied to remove unwanted frequencies while retaining the sample rate. In the end, the last 4 values per channel of each window are used as the extracted features for the classifier. In the current scenario, all features are normalized before they are used for classification.

Classification. Any kind of classification algorithm suited for binary decision tasks can be used here. We applied support vector machines with a linear kernel.

4.2 Experimental Setup

In this section the experimental setup which is used for the acquisition of both training and test data is presented.

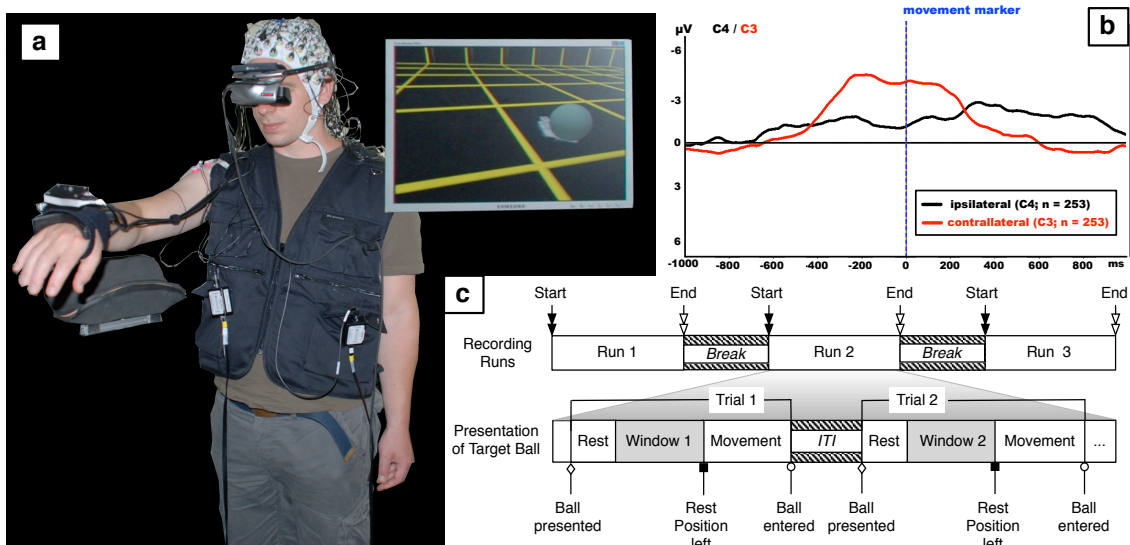


Figure 6: Experimental setup: a) Subject performs goal-oriented movements triggered by target balls; c) experimental design; b) averaged EEG activity before and after the movement measured above the primary motor cortex areas, ipsilateral (electrode position C4) and contralateral (electrode position C3) to the side of movement.

Subjects. Two subjects (two males, 30 and 27 years old) participated in this experiment. The participants were right-handed and had normal or corrected-to-normal vision. For each participant, three runs consisting of 60 trials were conducted on the same day, two of which were used for parameter optimization and one for validation.

Design and Procedure. Participants wore a head-mounted display (HMD) and stood in a dimly lit room while performing a task in a virtual environment. The task was to move their right arm from a rest position in order to reach virtual target balls, which were presented in the HMD to allow free movements independent of head position (Figure 6 a).

Leaving the rest position was detected by a hand-tracking system. Whenever the subjects moved their arm 5 cm away from the rest position, a marker for movement was sent and stored together with the EEG (Figure 6 b). Based on the movement marker, the EEG stream was segmented into windows of length of 1000 ms (Section 4.1).

After entering the target ball, the subjects returned to the rest position. At the same time the next target ball appeared. Time needed to return to the rest position and for the next target ball to appear depended on the distance between the entered target ball and the rest position. Therefore, this time, i.e. inter-trials-interval (ITI, Figure 6 c), varied according to the different distances between target balls and rest position.

To support the rest state of the arm, an armrest that was designed as part of our test bed was used.

This arm rest was integrated into the setup to imitate a strong support of the arm by the exoskeleton. This is for example useful whenever a subject is holding something still in his hand or is manipulating a device with outstretched arms. In both cases, a strong force would rest on the arm which the exoskeleton would support. Participants had to stay in the rest position for at least 5 seconds. In case that a subject would leave the rest position earlier, the next target ball would disappear. This was done to avoid too fast changes between movement and rest which was very important to assure long enough non-movement periods for training.

Data Acquisition. The EEG was continuously recorded from 128 electrodes (extended 10-20 system, actiCap, Brain Products GmbH, Munich, Germany), referenced to FCz. EEG signals were amplified using four 32-channel BrainAmp DC amplifiers (Brain Products GmbH, Munich, Germany) and filtered with a low cutoff of 0.1 Hz and high cutoff of 1000 Hz. Signals were digitized with a sampling rate of 5000 Hz. Impedance was kept below 5 k Ω .

5 RESULTS

In this section first results about performances in anticipating movements via the aBRI interface, and the suitability of the proposed control approach to modulate the exoskeleton joints impedance, are presented. It is worth to mention that tests of the two interfaces,

in this case, were conducted separately. Nevertheless this is sufficient to demonstrate the feasibility of our approach and gives solid basis to define future combined experiments.

5.1 Active Exoskeleton - Results

This section provides results for position and admittance control of hydraulic actuators using the schemes described in Section 3.2. Therefore, a single joint testbed was equipped with a hydraulic actuator driving a lever with a force sensor implemented at the tip. Actuator positions are acquired with an absolute optical encoder series *HEDS 9040* from Agilent providing a resolution of 2880 ticks per revolution, i.e. $\Delta q = \frac{0.125^\circ}{\text{tick}}$.

Position Control Results. For evaluating the position control performance of the testbed, a sequence of different desired positions is given within the workspace of $-84^\circ \leq q_d \leq 53^\circ$. For a better transient behavior, changes in reference are propagated to the control system by a PT^2 trajectory generator. See Figure 7 for results.

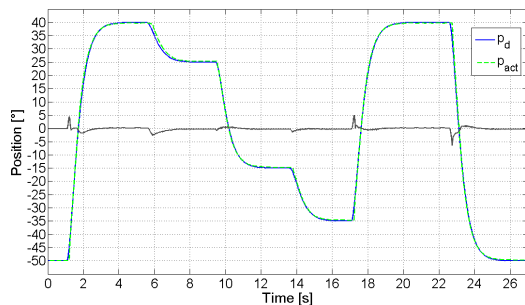


Figure 7: Single joint position results; solid: reference trajectory; dashed: actual joint position; grey: controller error.

The control loop shows a good performance in the overall working range. Desired positions are tracked with a steady state error of $e_{ss} = 0.25^\circ$ which is equal to two encoder ticks, while transients are followed by only a small phase shift. The precision of the control loop is limited to a minimum of one encoder tick. The maximum angular speed of the hydraulic actuator can be extracted to $\frac{dq}{dt} = \frac{90^\circ}{s}$.

The position controller offers a good positioning accuracy as well as a proper transient behavior and thus is a suitable basis for the tracking of a given trajectory.

Admittance Control Results. Here, the reaction of the admittance control system to a given input from

an operator is demonstrated. Furthermore, the influence of the stiffness and damping parameters K and D from Equation 2 on the behavior of the control loop is illustrated. For the first set of experiments only an adaption of K is performed, while damping is kept at a constant value. Afterwards, the damping is varied for a fixed stiffness. During all test runs, a human is trying to move the single joint along an identical trajectory from a start position of $q_d = -10^\circ$ (horizontal orientation of the lever) to an end position of $q_d = -30^\circ$ by exerting a force to the sensor located at the tip of the device.

Figure 8 depicts the results of piloting the joint in admittance control mode at different stiffness values and a constant damping of $D = 0.35$. Figure 8(a) shows the movement of the actuated joint, while Figure 8(b) presents the simultaneously measured contact forces. Note that the position trajectories are not aligned because they are performed manually by a human, trying to repeat the same movement in each run.

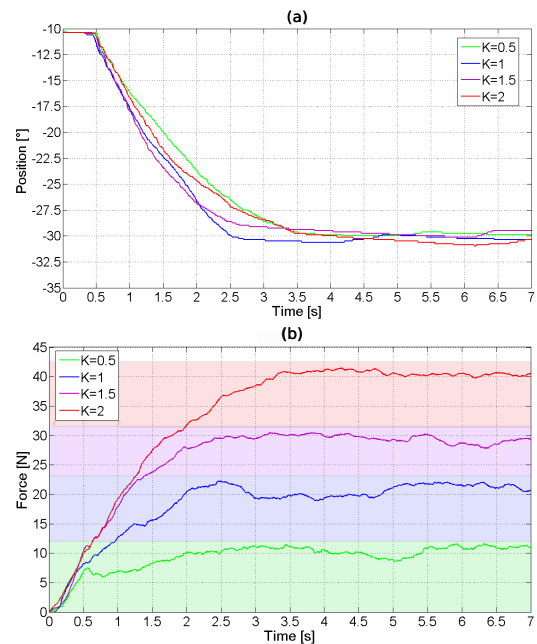


Figure 8: a) trajectories of hydraulic joint for different stiffness coefficients of admittance filter and constant damping of $D=0.35$; b) measured contact force between human and hydraulic actuator during the movements

It is obvious that an increase of the stiffness coefficient in the range of $K \in [0.5, 2]$ results in a higher contact force between operator and device during the whole movement, i.e. more force has to be generated by the user to transfer the system to the wanted position. Moreover, it can be determined that the steady state value for the contact force is directly proportional to K . Utilizing these results in the overall sce-

nario, the idea of lowering the stiffness according to a measured LRP will result in a smaller impedance of the device against performed motions, reduce the impact force at the beginning of the movement, and thus makes the device more transparent to the user.

In the next step, the influence of the damping coefficient D to the control loop is investigated, keeping the stiffness at a constant value of $K = 1$. Results of this experiment are depicted in Figure 9, while Figure 9(a) again shows the movement of the device, Figure 9(b) is containing the related force curves.

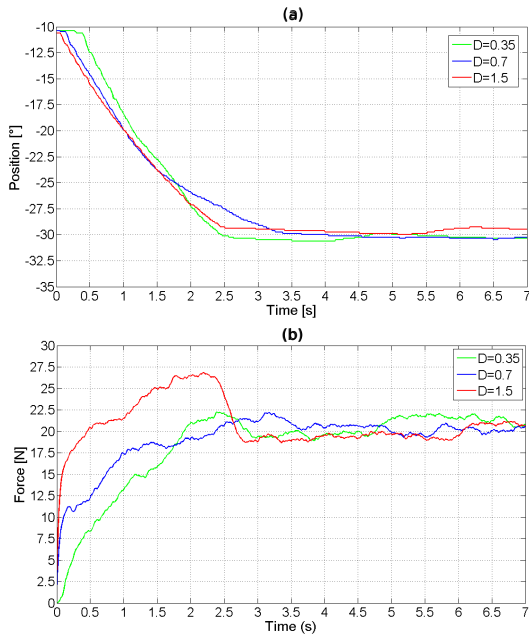


Figure 9: a) trajectories of hydraulic joint for different damping coefficients of admittance filter and constant stiffness of $K=1$; b) measured contact force between human and hydraulic actuator during the movements

By changing the damping ratio only the transient behavior is influenced, while the steady state values end up in the same interaction force governed by the stiffness coefficient. Mechanically damping can be described as a sink which dissipates more energy the higher it is. Experimental results verify this point of view by showing that the user has to apply more force for higher than for lower ratios, to get the device from the start to the end point in the same time.

5.2 aBRI - Movement Prediction Results

Three different analyses are presented below to outline our approach and to show current work. The aim of aBRI is to distinguish between the two classes:

“no movement” and “movement”. In contrast to various BCI-groups dealing with ERP research (Section 1), which often use *accuracy* as a performance measure of their systems, here *Area Under Roc* is applied. There are two reasons: first, the datasets are unbalanced (about four times more “no movement” instances) and second, even this class ratio might not be constant, e.g., in the online case. So a performance measure being robust against a varying class ratio has been chosen (Fawcett, 2006).

Data Processing Optimization Results. For the capability of the system to detect and respond to a movement preparation before its actual execution, both the classification performance and the running time of the data processing are important factors.

To get an impression which algorithms are applicable for online detection, the running time and the classification performance of several algorithms were measured and compared. A major bottleneck of the data processing are all operations that are applied before the decimation (which is the reduction of the sample rate with preceding filtering) since these have to deal with a high amount of data. In the used flow (Figure 5), these are the standardization and the anti-alias filtering step of the decimation itself.

To evaluate which algorithm is suitable for the filtering step decimation procedure, different anti-aliasing filters (AAF) were compared. All filtering steps of the AAF were applied in two consecutive steps (with decimation factors of 25 and 10, respectively). The inspected types were: the use of no filter at all (called *downsampling* in the following), a finite impulse response filter (FIR, applied as a direct form time domain convolution with a filter kernel having a length of 31 taps designed using the window design method and using a hamming window, omitting the time series values that are irrelevant due to the subsequent downsampling), and an elliptic infinite impulse response filter (IIR, with 60dB stopband attenuation with an order of 10, realized in direct form). Of the successive operations, the application of the band pass filter (BPF) was another time-consuming step, so that different types of BPF were examined (again with the described FIR and IIR filters, and simply using an FFT to set all unwanted frequencies to 0). For the evaluation of the classification performance, several high and low cutoffs of the BPF and several complexities (SVM parameter) were tested additionally.

Repeated measures ANOVA with four factors was performed: AAF (IIR, FIR, Downsampling), BPF (FFT, FIR, IIR), Low/High cutoff (0.4/4.0, 0.1/4.0, 0.4/2.0, 0.1/2.0) and SVM complexity (5.0, 1.0, 0.1, 0.01). Subsequently, repeated measures ANOVA with two factors was performed: AAF (IIR, FIR, Down-

sampling) and BPF (FFT, FIR, IIR, No). If needed, Greenhouse-Geisser correction was applied and the corrected p -value is reported. For pairwise comparisons, Bonferroni correction was applied.

A main effect of AAF [$F(2, 94) = 8.07, p < 0.005$; pairwise comparisons: IIR > Downsampling, IIR > FIR, Downsampling vs. FIR: n.s.] and a main effect of BPF [$F(2, 94) = 14.99, p < 0.001$; pairwise comparisons: FFT > FIR, IIR > FIR, FFT vs. IIR: n.s.] were found. There was an interaction between two factors [BPF x AAF: $F(4, 188) = 79.05, p < 0.001$]. Pairwise comparisons showed that the best combination was "IIR AAF-FFT BPF-0.1/4.0 Hz-0.1 complexity". Subsequent analysis of control condition (No BPF with three types of AAF) revealed that the best combination was significantly better than the control condition [$p < 0.002$].

Beside the classification performance, the computing time was evaluated. Even if the corresponding computations are performed on a high performance computing system in parallel, the used algorithms play an important role.

The running times are the averages of the wall-clock processing times of windows of all datasets that were used in the optimization procedure. We used an Apple Mac Pro with two Intel Quad-Core Xeon processors (resulting in 16 virtual cores due to Hyper-Threading) at 2.66 GHz and 32 GB memory for the time measurements. A channel-wise parallelization of the used filtering procedures and the standardization was performed using OpenMP. The average and maximum running times are shown in Table 1.

Table 1: Average (and maximum computation times in brackets) of different filtering algorithms in ms.

Anti alias filter type	Band pass filter type			
	FIR	IIR	FFT	No
FIR	26.4 (64.3)	25.4 (30.6)	28.0 (34.5)	20.3 (24.5)
IIR	25.4 (28.4)	24.9 (28.0)	27.6 (31.6)	20.2 (27.1)
No	20.7 (25.0)	19.8 (26.6)	22.4 (29.9)	14.7 (21.5)

Time-Dependent Classification Performance.

Apparently, the longer the distance in time between classification and actual movement onset, the more difficult it is for the algorithm to detect the BP/LRP. In addition neurobiological analysis about the beginning of movement preparation from averaging lots of trials for the channels C3 and C4 (Figure 6 c) does not allow to draw conclusions for the multi-channel single trial case. To obtain knowledge about how performance increases with sliding in

time closer to the movement, a 5×2 cross-validation with the optimized parameters on one dataset of each subject was performed. These datasets were not used for the optimization procedure to ensure reliable performance measurements.

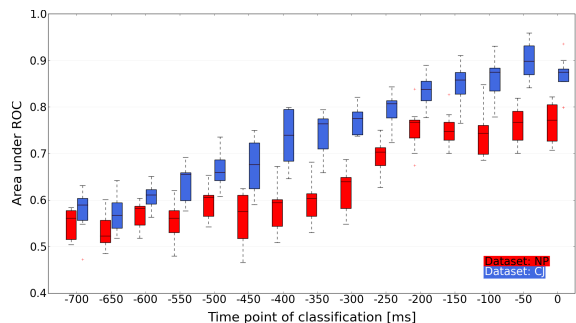


Figure 10: Boxplots of the time-dependent classification performance for two subjects: NP (red) & CJ (blue).

Figure 10 shows the evolution of performance over time, whereas the time points denote the end of each extracted time window. I.e., one box plot depicts the result for a classifier trained on windows up to a specific time point and tested on other trials windowed with the same procedure. Note that the movement marker (time point zero) does not indicate movement onset, since it is stored when the subject had already moved 5 cm. That means, the interesting range for the brain-arm interface would be quite before that point (at least around -150 to -250 ms).

Although, in the online case, there is no time-dependent classification possible and also the subject-specific differences need further investigations, these results demonstrate that the approach in principle allows to detect movement preparation.

Online Simulation Results. Since, in the real applicable system, there will be a continuous movement prediction, another test was conducted on the same datasets as for the time-dependent test, but this time in an pseudo online manner. For the test, a classifier with optimized parameters was trained on two different windows of each trial, i.e., cut out up to -250 and -150 ms. This was done to make the classifier somehow robust (Blankertz et al., 2006) against the "moving" LRP in the windows. The classifier is then tested on sliding windows extracted every 50 ms.

For the "Force Control" module of the brain-arm interface, a continuous value S_{LRP} from 0 to 1 is expected. To achieve this, the SVM score can be used and scaled in the demanded range. In Figure 11, the classifier output against the time point of classification is shown. It is below zero if an instance is classified to be "no movement" and above zero otherwise.

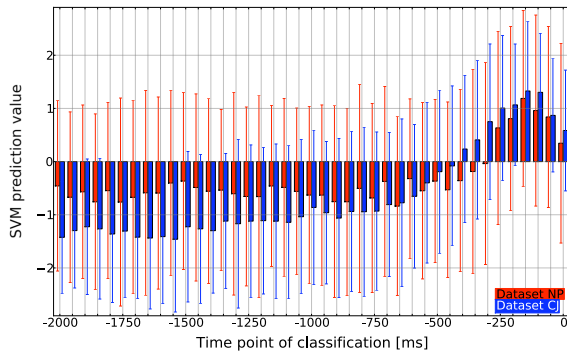


Figure 11: Mean (bars) with standard deviation (errorbars) of the SVM prediction values for sliding windows of the test datasets of two subjects: NP (red) & CJ (blue).

Scaling can be done for example by

$$S_{LRP} = \begin{cases} svm_{min} & \text{if } svm_a < svm_{min} \\ \frac{svm_a}{2 \cdot svm_{max}} + 0.5 & \text{if } svm_a \in [svm_{min}, svm_{max}] \\ svm_{max} & \text{if } svm_a > svm_{max} \end{cases}$$

where svm_a is the SVM score for the actual classified time window in the online test case and svm_{min} & svm_{max} are the minimum and maximum values for the SVM score obtained in the training phase of the classifier.

6 CONCLUSIONS AND FUTURE WORK

This paper proposes the architecture of a multimodal haptic interface that has two main fields of application: as a control device to operate complex and heterogeneous robotic systems in an intuitive manner, and as rehabilitation tool in order to facilitate and speedup the recovery procedure of upper limbs. In particular a control scheme that combines bio-inspired with classical control techniques, and integrates information about movements preparation, is presented. In comparison to classical BCI approaches, the proposed aBRI interface does not use brain signal, to directly control the movements of the haptic device, on the contrary the information is used to modulate its impedance and therefore to facilitates the prepared user movements. This improves the natural feeling in wearing the interface, enhancing the operation of the robotics system, and increasing the quality of the therapy.

Results show that modulating the stiffness and damping of the force controller can be used on one hand to ensure a safe interaction in case of low LRP detection scores, by avoiding a too sensitive reaction

to motion inputs from the operator. On the other hand, this feature can be used to facilitate the ability of the system to work as a rehabilitation device, resisting or supporting the movements of a user.

For future work we plan to improve performance of the movement prediction by e.g., investigating several other classification and data processing algorithms, perform a thorough evaluation of filter algorithms and further smoothing methods, as well as combining the detection of ERPs and changes in the frequency range. Further on, we will improve adaptability to different users and changes in brain activity during the usage by the development of self-adapting methods for aBRI.

Finally experiments that combine both interfaces (Exoskeleton, aBRI) have to be conducted, this in order to demonstrate the feasibility of the proposed control approach in a real time scenario. Questions relatively the user comfort and the benefits of the on-line joint stiffness modulation have to be addressed via testing the system on different users.

REFERENCES

- Balconi, E. (2009). The multicomponential nature of movement-related cortical potentials: functional generators and psychological factors. *Neuropsychological Trends*, 5:59–84.
- Blankertz, B., Curio, G., and Müller, K. (2002). Classifying single trial EEG: Towards brain computer interfacing. In *Advances in neural information processing systems 14: proceedings of the 2001 conference*, pages 157–164. MIT Press.
- Blankertz, B., Dornhege, G., Lemm, S., Krauledat, M., Curio, G., and Müller, K. (2006). The Berlin Brain-Computer Interface: Machine learning based detection of user specific brain states. *Journal of Universal Computer Science*, 12(6):581–607.
- Blankertz, B., Dornhege, G., Schäfer, C., Krepki, R., Kohlmorgen, J., Müller, K., Kunzmann, V., Losch, F., and Curio, G. (2003). Boosting bit rates and error detection for the classification of fast-paced motor commands based on single-trial EEG analysis. *IEEE Transactions on Neural Systems and Rehabilitation Engineering*, 11(2):127.
- Farwell, L. and Donchin, E. (1988). Talking off the top of your head: toward a mental prosthesis utilizing event-related brain potentials. *Electroencephalography and clinical Neurophysiology*, 70(6):510–23.
- Fawcett, T. (2006). An introduction to ROC analysis. *Pattern recognition letters*, 27(8):861–874.
- Folgheraiter, M., Bongardt, B., Albiez, J., and Kirchner, F. (2009a). Design of a bio-inspired wearable exoskeleton for applications in robotics. In *International Joint Conference on Biomedical Engineering Systems and Technologies (BIOSSTEC-2009)*, Portugal, Porto.

- Folgheraiter, M., Bongardt, B., de Gea Fernández, S. S. J., Albiez, J., and Kirchner, F. (2009b). Design of an arm exoskeleton using an hybrid motion-capture and model-based technique. In *IEEE International Conference on Robotics and Automation (ICRA-2009)*, May 12-17, Kobe, Japan.
- Folgheraiter, M., de Gea, J., Bongardt, B., Albiez, J., and Kirchner, F. (2009c). Bio-inspired control of an arm exoskeleton joint with active-compliant actuation system. *Applied Bionics and Biomechanics*, 6(2):193–204.
- Harwin, W., Patton, J., and Edgerton, V. (2006). Challenges and opportunities for robot-mediated neurorehabilitation. *Proceedings of the IEEE*, 94(9):1717–1726.
- Hogan, N. (1985). Impedance control - an approach to manipulation. i - theory. ii - implementation. iii - applications. *ASME Transactions Journal of Dynamic Systems and Measurement Control B*, 107:1–24.
- Jones, E., Oliphant, T., Peterson, P., et al. (2001). SciPy: Open source scientific tools for Python.
- Kirchner, E. A., Metzen, J. H., Duchrow, T., Kim, S., and Kirchner, F. (2009). Assisting telemanipulation operators via real-time Brain Reading. In *Lemgoer Schriftenreihe zur industriellen Informationstechnik*, Paderborn.
- Kirchner, E. A., Wöhrle, H., Bergatt, C., S. K. Kim, J. H. M., and Kirchner, F. (2010). Towards operator monitoring via brain reading - an eeg-based approach for space applications. In *Proceedings of the 10th International Symposium on Artificial Intelligence, Robotics and Automation in Space*.
- Kornhuber, H. and Deecke, L. (1965). Hirnpotentialänderungen bei Willkürbewegungen und passiven Bewegungen des Menschen: Bereitschaftspotential und reafferente Potentiale. *Plügers Archiv für die gesamte Physiologie des Menschen und der Tiere*, 284:1–17.
- Krauledat, M., Dornhege, G., Blankertz, B., Curio, G., and Müller, K. (2004). The Berlin brain-computer interface for rapid response. *Biomedizinische Technik*, 49(1):61–62.
- Krebs, H. I., Ferraro, M., Buerger, S. P., Newbery, M. J., Makiyama, A., Sandmann, M., Lynch, D., Volpe, B. T., and Hogan, N. (2004). Rehabilitation robotics: pilot trial of a spatial extension for mit-manus. *Journal of Neuroengineering and Rehabilitation*, 1(1):5.
- Leeb, R., Keinrath, C., Friedman, D., Guger, C., Scherer, R., Neuper, C., Garau, M., Antley, A., Steed, A., and Slater, M. (2006). Walking by thinking: the brainwaves are crucial, not the muscles! *Presence: Teleoperators and Virtual Environments*, 15(5):500–514.
- Li, Y., Gao, X., Liu, H., and Gao, S. (2004). Classification of single-trial electroencephalogram during finger movement. *IEEE Transactions on biomedical engineering*, 51(6):1019–1025.
- Masaki, H., Wild-Wall, N., Sangals, J., and Sommer, W. (2004). The functional locus of the lateralized readiness potential. *Psychophysiology*, 41(2):220–230.
- Mistry, Mohajerian, and Schaal (2005). Arm movement experiments with joint space force fields using an exoskeleton robot. In *9th International Conference on Rehabilitation Robotics*.
- Pires, G., Nunes, U., and Castelo-Branco, M. (2007). Single-trial EEG classification of movement related potential. In *IEEE 10th International Conference on Rehabilitation Robotics, 2007. ICORR 2007*, pages 569–574.
- Reinkensmeyer, D., Lum, P., and Winters, J. (2001). Emerging technologies for improving access to movement therapy following neurologic injury. *Emerging and Accessible Telecommunications*.
- Reinkensmeyer, D. J., Emken, J. L., and Cramer, S. C. (2004). Robotics, motor learning, and neurologic recovery. *Annual review of biomedical engineering*, 6:497–525.
- Rosen, J., Perry, J., Manning, N., Burns, S., and Hannaford, B. (2005). The human arm kinematics and dynamics during daily activities - toward a 7 dof upper limb powered exoskeleton. In *Advanced Robotics, 2005. ICAR '05. Proceedings., 12th International Conference on*, pages 532–539.
- Sajda, P., Gerson, A., Muller, K., Blankertz, B., and Parra, L. (2003). A data analysis competition to evaluate machine learning algorithms for use in brain-computer interfaces. *IEEE Transactions on neural systems and rehabilitation engineering*, 11(2):184–185.
- Schiele, A. and van der Helm, F. (2006). Kinematic design to improve ergonomics in human machine interaction. *IEEE Transactions on neural systems and rehabilitation engineering*, 14(4):456–469.
- Squires, N., Squires, K., and Hillyard, S. (1975). Two varieties of long-latency positive waves evoked by unpredictable auditory stimuli. *Electroencephalography and clinical Neurophysiology*, 38(4):387–401.
- Wolpaw, J., Birbaumer, N., McFarland, D., Pfurtscheller, G., and Vaughan, T. (2002). Brain-computer interfaces for communication and control. *Clinical neurophysiology*, 113(6):767–791.
- Zito, T., Wilbert, N., Wiskott, L., and Berkes, P. (2008). Modular toolkit for data processing (mdp): a python data processing frame work. *Front. Neuroinform.*, 8(2).